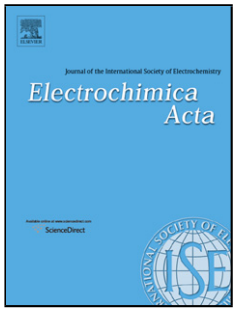

Title: Investigation of the oxygen reduction reaction on Pt-WC/C electrocatalysts in alkaline media

Author: Amanda C. Garcia Edson A. Ticianelli

PII: S0013-4686(13)01068-2
DOI: http://dx.doi.org/doi:10.1016/j.electacta.2013.05.128
Reference: EA 20618

To appear in: *Electrochimica Acta*

Received date: 18-2-2013
Revised date: 6-5-2013
Accepted date: 28-5-2013

Please cite this article as: A.C. Garcia, E.A. Ticianelli, Investigation of the oxygen reduction reaction on Pt-WC/C electrocatalysts in alkaline media, *Electrochimica Acta* (2013), http://dx.doi.org/10.1016/j.electacta.2013.05.128

Investigation of the oxygen reduction reaction on Pt-WC/C electrocatalysts in alkaline media

Amanda C. Garcia, Edson A. Ticianelli

Instituto de Química de São Carlos, Universidade de São Paulo, Avenida Trabalhador Sãocarlense, 400 Parque Arnold Schmidt, CP 780 13560-970 São Carlos, SP, Brazil

Abstract

The activity of Pt catalysts dispersed on tungsten carbide (WC) prepared with a high surface area carbon with two different WC/C ratios is investigated for the oxygen reduction reaction (ORR) in alkaline electrolyte. The electrochemical methods employed are cyclic voltammetry (CV) and steady-state polarization carried out on an ultrathin catalyst layer deposited on the disk of a rotating ring–disk electrode. The PtWC-based catalysts show higher activity for the ORR compared to Pt/C, also involving a transfer of 4 electrons per oxygen molecule. CV and X-ray absorption near edge structure spectroscopy (XANES) results for the PtWC-based materials indicate weaker Pt-OH_x interaction in these materials, resulting in a lower Pt-oxide coverage and explaining the increased rate of the ORR, as compared to Pt/C

Key words: PtWC/C electrocatalysts, oxygen reduction reaction, alkaline fuel cell, in situ XANES.

Corresponding author: Dr. Amanda C. Garcia (amandagarcia@iqsc.usp.br),

phone: ++ 55 16 3373 9934 fax: ++ 55 16 3373 9952

1. Introduction

Fuel cell technology is expected to become an important source of clean electric power, particularly for motorized vehicules [1]. However, considerable advances and significant improvements in existing fuel-cell technology are still necessary [2], especially in relation to the oxygen reduction reaction (ORR), which plays a pivotal role, because the corrosive conditions of the fuel-cell cathode require chemically stable noble catalysts cathode, active enough to activate O_2 and then release it in the form of H_2O. Platinum cathodes are the more effective electrocatalyst for the ORR under acid or alkaline conditions [3]. Hence, studies aimed at reducing the amount of noble metal in the cathode are still attractive. It has been widely observed that Pt alloys such as Pt–V, Pt-Cr, Pt–Co [4] and Pt-Fe [5] show better kinetics for the ORR than pure Pt. This improvement is usually assigned to changes in the electronic properties of Pt in the alloys, as induced by the non noble metal [6].

Among the many materials developed for application in the cathode of the fuel cell, transition metal carbides has attracted a lot of attention, since they show some activity to catalyze different types of reaction, either in the absence or in the presence of metallic nanoparticulated catalysts [7]. Examples of such reactions are the hydrogen evolution reaction investigated on bare carbides (WC, W_2C and Mo_2C) [7,8], the methanol and hydrogen oxidation reactions promoted on tungsten carbides or tungsten carbide/carbon (WC/C) composites [7,9] and on Pd, Pd-Ni and Pt supported WC or WC/C catalysts [10-12]; and finally the oxygen reduction reaction investigated on Pt, Pt-alloys and Pd-Au supported on WC or WC/C, either in liquid acid [13-16] or alkaline [17-21] electrolytes, and on the polymer electrolyte fuel cell cathode environment [15,22]. Results obtained for the oxygen reduction reaction in acid electrolytes in Pt-WC/C catalysts show that they present higher activity for the

ORR, as compared to Pt supported on carbon (Pt/C), but this is not a consensus [14,20]. In alkaline electrolytes, the literature related to the ORR electrocatalysis on WC/C or Pt-WC/C is scarce [17,19-21], but here the activity of bare WC/C for this reaction is quite pronounced [13], contrarily what is found in acid media. The beneficial effect of WC/C on Pt seems to be clearly observed in alkaline media [17,20,21] including the case where pure single nanocrystalline tungsten carbide has been employed to prepare the Pt-WC/C electrocatalysts [20]. In this case one third Pt loading, compared to Pt/C, showed improved kinetics and onset potential for ORR.

A question which remains unclear is the mechanism by which the improvement in the ORR electrocatalysis is achieved. Although it has been already suggested that an electron exchange between Pt and WC [14,22], leading to a rearrangement of the Pt d-band, similarly to the effect of alloying Pt with non-noble metals, may be the reason for this effect, no direct results are available to support this proposal. In this work, the electrocatalytic performance of platinum catalysts supported on tungsten carbides (Pt-WC/C) prepared by a sonochemical method, was investigated for the ORR in alkaline medium. Chemical and physical properties of the materials were assessed by energy dispersive X-ray analysis (EDX), X-ray diffraction (XRD) and transmission electron microscopy (TEM). Cyclic voltammetry (CV) and steady-state polarization curves for the ORR were investigated on ultra-thin catalyst layer deposited on the disk of a rotating ring-disk electrode (RRDE). Changes in the electronic properties of Pt caused by the presence of tungsten carbides were characterized by X-ray absorption near edge structure (XANES) spectroscopy at the Pt L_3 edge.

2. Experimental section

2.1 Preparation of the tungsten carbides

Preparations of tungsten carbides with two different atomic ratios (WC/C) were carried out by a procedure earlier described for molybdenum carbide [23]. For this, a slurry of tungsten hexacarbonyl (1 g in 50 mL of hexadecane) and the desired amount of a carbon powder (Vulcan XC-72R) was ultrasonic treated in a high-intensity ultrasonic bath (Unique, 0.5 in Ti horn, 19 kHz, 80 W cm^{-2}) at 90 °C for 3 h under argon, to produce a black powder slurry. After, the solid was filtered and the powder washed three times with pure degassed pentane, and finally heated at 100 °C. To prevent tungsten oxide interfering with catalytic activity, they were carburized before the catalytic tests by heating in a flow of 1:1 CH_4/H_2 at 300 °C for 1 h, then at 400 °C for 1 h and finally at 500 °C for 12 h. Excess carbon, hydrogen and oxygen were largely removed by this treatment [24].

2.2 Preparation of the tungsten carbide supported Pt electrocatalysts

Chloroplatinic acid (H_2PtCl_6), water and previously prepared WC/C were mixed and treated in an ultrasonic bath, to form a uniformly dispersed ink. This was heated to 80 °C and the platinum was then reduced with formic acid solution [25], added slowly with stirring. The mixture was filtered and the powder washed several times with purified water and finally dried at 80 °C for 1 h. Nominal composition were 20 wt.% of Pt with respect to the WC/C weight.

2.3 Chemical and physical characterizations

The atomic ratios of the Pt-WC/C, Pt/C, and WC/C electrocatalysts were determined by EDX analysis conducted with 20 keV electron beam in a scanning electron microscope (DSM 960 Zeiss) equiped with a Link Analytical QX 2000

microanalyzer and a SiLi detector. X-ray diffraction patterns were collected with a Rigaku Rotaflex RU-200B diffractometer using Cu Kα radiation (λ=0.15406) generated at 40 *k*V and 20 mA. Scans were conducted at 2° min^{-1} for 2θ in the range 20 to 100°. The average crystallite size was calculated by Scherrer's equation [26]:

$$d = k\lambda / B \cos \theta \quad (1)$$

where d is the average crystallite size in *Å*, k a coefficient taken here as 0.9, λ the wavelength of the X-rays used (1.5406 *Å*), B the width of the diffraction peak at half height in radians, and θ the angle at the position of the peak maximum. For this purpose, the (220) peak at 2θ = 68° of the Pt face-centered cubic (fcc) structure was used. To improve the fitting quality of this peak, the XRD pattern for 2θ values from 60 to 80° was recorded at 0.02° min^{-1}.

For the TEM experiments, cooper-coated grids were immersed into the Pt-WC/C-based suspensions and allowed to dry overnight in a desiccator. The samples were analyzed in a TEM FEI Tecnai equipment at an accelerating voltage of 200 kV.

2.4 Electrochemical measurements

For the electrochemical measurements a rotating disk, a platinum foil and $Hg/HgO/OH^-$ in 1.0 M KOH were employed as working, counter and reference electrodes, respectively. A glassy carbon disk (ϕ = 5 mm, geometric area = 0.196 cm^2) was used as the substrate to prepare the active layers of Pt-WC/C, Pt/C, and WC/C. These layers were prepared by suspending 2.0 mg of the catalytic powder in a mixture of 1 mL of isopropyl alcohol and 20 μL of a Nafion solution (5 wt % in low aliphatic alcohol, from DuPont) and ultrasonicated to an homogeneous ink. 20 μL of this ink was droped onto the glassy carbon disk and allowed to dry at ambient temperature.

The total Pt amount deposited over the substrate was 0.04 mg, for electrocatalysts containing the noble metal.

The experiments were conducted in 1.0 M KOH (99.99 %, Aldrich) prepared with ultrapure water from a Milli-Q (Millipore) system. In 1.0 M KOH the diffusion coefficient D, the solubility C^* of the oxygen in the electrolyte and the kinematics viscosity v are respectively, 1.56 x10^{-5}, 8.8 x10^{-4} and 1.9 x10^{+3} [28]. The electrolyte was saturated with purified N_2 or O_2, depending on the experiment. Voltammetric curves were recorded, in the range of potentials from – 0.88 to 0.2 V *vs.* Hg/HgO/OH^-, with an AUTOLAB potentiostat (PGSTAT30). All the experiments were conducted under N_2 at room temperature (25 °C).

Steady-state polarization curves were recorded at 5.0 mV s^{-1} with the RRDE rotation at range speeds 400 to 3600 rpm to assess the ORR kinetics. In these experiments, the disk and the ring currents were recorded as the potential was varied between 0.1 and – 0.7 V *vs.* Hg/HgO/OH^-, using an AUTOLAB bipotentiostat (PGSTAT30). The Pt ring electrode was employed to sense the HO_2^- generated on the working disk electrode (described above) by the ORR. This was made by measuring the magnitude of the HO_2^- oxidation current at the ring electrode placed at a potential of 0.2 V *vs.* Hg/HgO/OH^-: this potential is sufficiently high to ensure the complete oxidation of any HO_2^- ions reaching the ring by centrifugal flow due to the rotation of the disk, while sufficiently low to hinder any O_2-evolution reaction. As a result, only the HO_2^- oxidation reaction could occur on the platinum ring. The ring (I_R) and disk (I_D) currents were measured simultaneously and plotted against the disk potential E_D.

The collection efficiency, $N = I_R/|I_{D2e\text{-}}|$, namely the percentage of HO_2^- ions formed on the disk which are detected on the ring, was determined for the RRDE electrode from the slope of the ring-current *vs.* disk-current plot at various rotation rates, using classical redox couple $Fe(CN)_6^{3-}/Fe(CN)_6^{4-}$ [29], in an electrolyte solution

of 10^{-2} M of $K_3Fe(CN)_6$ in 0.5 M H_2SO_4. A value of N equal to 0.36 was found. This value was used to determine the extent of peroxide formation and the number of electron (n_t) exchanged per reduced O_2 molecule in the course of the ORR. This was calculated in the ORR potential range from the measured disk currents I_D, the ring current for peroxide oxidation I_R and the collection efficiency N, by using equation 2 [30]:

$$n_t = \frac{4\,|I_D|}{|I_D| + (I_R/N)} \qquad (2)$$

while, the molar proportion of HO_2^- ions formed on the disk (x^m) was determined from the n_t values, according to the procedures described in refs [30,31] and equation 3:

$$x^m = \frac{n_{HO2-}}{n_{O_2}} = \frac{(4 - n_t)}{2} \qquad (3)$$

2.5 Electronic properties of Pt

The materials were also characterized as *in situ* electrodes by X-ray absorption spectroscopy (XAS) in the XANES region, from measurements performed at the Pt L_3 absorption edge (11564 keV). The *in situ* measurements refer to the XANES spectra obtained with the electrode maintained at desired potentials. For these measurements, an acrylic electrochemical cell with an aperture to allow the X-ray beam passage was employed [32]. The cell contained three electrodes, a working electrode, a Hg-HgO/OH^- reference electrode and a platinum mesh as the counter electrode.

The measurements were made on working electrodes consisting of pellets formed out of the dispersed catalysts bound with Nafion (5 wt.%) with a metal (Pt) load of 6 mg cm^{-2}. These measurements were made at -0.3 V and -0.03 V *vs.* Hg-HgO. The experiments were conducted in 1.0 M KOH (99.99 %, Aldrich) prepared with ultrapure water from a Milli-Q (Millipore) system. All XANES experiments were carried out at the D04B-XAFS1 beam line in the National Synchrotron Light Source Laboratory (LNLS), Brazil. X-ray absorption spectra were collected with three ionization chambers (incidence I_0, transmitted I_t, and reference I_r). The reference channel was used mainly to calibrate the edge position, with a pure Pt foil sample. The computer program WinXAS was used to analyze the XAS data. Further details can be found in the literature [27].

3. Results and Discussion

3.1 Characterization of the Bulk Composition

EDX results showed that the experimental percentage of tungsten carbide are near to the nominal values, which were 20 and 60 wt. %. EDX was also used to determine the amounts of platinum in the Pt/C and PtWC-based catalysts and these were very close to the nominal value of 20 wt. %. In order to identify the various materials, the following nomenclature will be used: the PtWC catalyst synthesized with 20 wt. % WC/C will be denoted as Pt- 20 WC/C and the PtWC catalyst synthesized with 60 wt. % WC/C will be denoted as Pt- 60 WC/C.

The different catalysts were analyzed by XRD, as shown in Fig. 1. The peaks in curves d and e confirm that the samples were mixtures of mono-tungsten carbide

(WC) and di-tungsten carbide (W_2C). The presence of W_2C was probably due to the quite low temperatures used for the carburization with CH_4/H_2 [24]. These XRD results are consistent with published data [33]. The XRD patterns confirm the presence of the face-centered cubic (fcc) structure typical of platinum metal, in the Pt/C and PtWC-based catalysts (curves a, b and c). For both PtWC catalysts (curves b and c), the Pt diffraction peaks are slightly shifted to higher angles compared to those of the Pt/C electrocatalyst. This evidences a slight contraction of the unit cell, as confirmed by the lattice parameters in Table 1, which is an indication of some interaction between Pt and the WC composites. Also, curves b and c did not show any peak related to WC and so it may be assumed that some of the W atoms must be in the form of a segregated amorphous WO_x phase mixed with the carbon support. The occurrence of some alloying of Pt with W is perhaps also occurring, as evidenced by the contraction of the Pt lattice parameters (Table 1) in the PtWC electrocatalysts. In any case, these phenomena indicate that the carbide structures initially present in the substrate may suffer some changes during the Pt deposition process.

The broad Pt peaks denote very small Pt crystallites and that these were highly dispersed on the carbon. The average Pt crystallite sizes for all catalysts were calculated using the Scherrer equation (1); these were 3.0, 5.0 and 5.3 nm for Pt/C, Pt-20WC/C and Pt-60WC/C, respectively, as shown in Table 1.

TEM images of the Pt-20WC/C nanoparticles are shown in Fig. 2a. These micrographs indicate that the Pt nanoparticles are in the form of small spheres highly dispersed on the substrate. Similar results were obtained for Pt-60WC/C catalysts (Fig. 2b); in these cases, the nanoparticle sizes are in the range of 7 nm to 9 nm for Pt-20WC/C and Pt-60WC/C, respectively. It is noted that the particle sizes obtained by XRD were lower than those obtained by TEM, and this evidences that the particles observed by TEM in fact correspond to agglomerated crystallites. In this way, the

results clearly denote higher Pt particle sizes (low surface areas) in the Pt-carbide materials.

3.2 Electrochemical measurements

Fig. 3 shows CV profiles for the different materials with the currents normalized per geometric area of the carbon disc substrate. For the 20WC/C no redox peaks were observed in the range of potential in alkaline solution under ambient temperature. For 60WC/C (not shown) similar results were observed over the whole voltammogram.

The results in Fig. 3 for the Pt-based electrocatalysts also show typical behavior regarding the hydrogen and oxide regions on Pt in alkaline solution [28]. In the case of the Pt-WC/C (20 and 60 wt. %) electrocatalysts the peaks in the hydrogen region are well resolved and very similar to those for Pt/C, although they present smaller magnitudes, consistent with smaller Pt surface areas, as also shown by XRD and TEM. In the oxide region, Fig. 3 evidence a small shift to anodic direction of the platinum oxide reduction peak position for the Pt-tungsten carbide catalysts, compared to Pt/C. Such effect be can attributed to a decrease of the desorption free energy of Pt-OH, Pt-O or Pt-O_2 due to presence WC/C, so that the reduction of intermediates containing oxygen becomes more facile.

The active area of the Pt-based catalysts, calculated from the hydrogen desorption charges of the cyclic voltammograms [34], are shown in Table 1. Values of surface areas for the PtWC materials obtained by TEM, assuming spherical particles, and by XRD are also included in this Table 1. The values of the active areas obtained with the three techniques show that the active area for Pt-WC catalysts are lower than that of Pt/C, and this result is in agreement with the lower magnitude of

the peaks observed in the hydrogen region of the CV (Fig. 3). However, the active areas obtained by TEM and XRD for the PtWC catalysts resulted in higher values compared to those obtained by CV, indicating that the utilization of Pt is smaller than 100 %, as expected due to the loss of Pt area in the regions of close contact of the particles with carbon of WC/C.

3.3 ORR measurements

Fig. 4a and 4b show the HO_2^- oxidation currents in the ring and the steady-state polarization curves for oxygen reduction on the disc, respectively, for the Pt-60WC/C electrocatalyst, at several rotation rates. The onset potential for oxygen reduction is about 0.06 V and the mass-transport limited current regions are evident from – 0.15 to -0.7 V. The corresponding results for the various materials at 1600 rpm are compared in Figs. 4c and 4d. It is noted that the ORR limiting current densities assume close values for the Pt/C and the PtWC-based catalysts. This is in agreement with an ORR mechanism involving preponderantly the four-electron route, which leads to the formation of OH^- ion [28]. Lower values of limiting currents are observed for WC/C (20 and 60 %), close to the values obtained for Vulcan carbon. This implies that, for these catalysts, the reaction may take place in the WC/C phase and also in the carbon support, involving a parallel route via two-electrons leading to the formation of peroxide ion, as proposed earlier [35] for other Pt-based electrocatalysts.

The number of electrons involved in the ORR and the molar proportion of HO_2^- were calculated by equations 2 and 3, respectively, for all catalysts, and the values are included in Table 2. These results show that for all Pt-based catalysts the values of n_t are close to 4 electrons per oxygen molecule, showing that these materials reduce oxygen by the 4 e^- pathway, as also evidenced by the low peroxide oxidation

currents (Fig. 4c) and the molar ratios of HO_2^- ions reported in Table 2. For the Vulcan carbon and the WC/C (20 and 60 %) catalysts the results presented in Fig. 4c show a higher rate of H_2O_2 formation than for the Pt-based materials. The molar ratios of HO_2^- (x^m / %) ions were found to be 91.0, 65.0 and 25.0, for the Vulcan carbon, WC/C (60 and 20 %), respectively, and these values are consistent with the number of electrons transfered per oxygen molecule, 2.2, 2.5 and 2.7, respectively. These results are in accordance with values reported previously for some carbon supported Pt-based materials [36].

Fig. 4c and 4d and also Table 2 show that for the Pt-60WC/C and Pt-20WC/C electrocatalysts, the onset potential of the ORR shifts to values around 50 mV and 30 mV more positive, respectively, compared to Pt/C, evidencing the higher activity of these materials, in agreement with is often observed in the literature for the ORR in alkaline media [17,19-21]. This enhancement of the ORR may be assigned to several factors, including changes in the electronic properties of Pt caused by the presence of the tungsten carbides, in the degree of coverage of oxide surface layers on Pt, and in the surface areas.

A more specific comparison of the catalytic activities were made from the values of the specific activities (SA) toward the ORR at -0.076 V and -0.026 V (vs. Hg/HgO/OH^-). These values (Table 3) were calculated dividing the ORR currents at these electrode potentials by the real Pt electrode surface area, as obtained by CV. Results in Table 3 confirm that the specific activities of the Pt-60WC/C and the Pt-20WC/C electrocatalysts are higher than that of Pt/C, with the Pt-60WC/C material showing slightly higher performance

Results of XRD, HRTEM and CV indicate that the Pt surface areas are in fact smaller in the Pt-carbide materials, a tendency which is contrary to the observed catalytic effect based in the geometric area (or equivalently, the mass of the Pt

catalyst). To verify the electronic effect of the tungsten carbide on the platinum properties, *in situ* XANES analyses were carried out and the results are shown in Fig. 5 for the PtWC-based catalysts, in comparison with those for Pt/C. XANES spectra were recorded at the Pt L_3 edge for samples at -0.3 V and -0.03 V vs. Hg/HgO/OH^-. At the Pt L_3 edge (11564 eV), absorption corresponds to the $2p_{3/2}$ to 5d transitions, with the magnitude of the absorption peak or white line located at ca. 5 eV above the edge being directly related to the Pt 5d electronic occupancy. A higher peak corresponds to a lower occupancy, and vice-versa [37]. For the W-based catalysts a pre-edge feature at the W L_2 edge is seen, most probably involving WC and/or WO_x species [38]. The magnitudes of this absorption hump are in agreement with the W loads in the samples.

It should be noted that the only unoccupied *d* level in the Pt atom is the $5d_{5/2}$ state and only the L_3 edge makes transitions to such a final state, since it originates from a $p_{3/2}$ state. The electronic transition at the L_2 edge is originated from the $p_{1/2}$ state, and thus only involves Pt $5d_{3/2}$ and s final states. In the metallic form the lack of a white line at L_2 [22] and its presence at L_3 can be understood by assuming that the holes in the d band retain the $d_{5/2}$ character. So, as a conclusion only the L_3 edge would be relevant to investigate the occupancy of the Pt 5d band, and this is the reason why this edge was used in this work despite of the existence of some interference of the W L_2 edge.

Fig. 5a and 5b show that the white line magnitude increase with the increase of the electrode potential for the Pt/C catalyst in alkaline medium. This is well know phenomenon which is attributed to the emptying of the 5d band, caused by an electron withdrawing effect of the oxygen present in the surface oxide layer formed above -0.1 V on the catalyst particle surface. From Fig. 5a it is seen that at -0.3 V (corresponding to a potential in the double layer region of Pt) the magnitudes of the white line are

essentially the same for the different catalysts, although for Pt-60WC/C the white line magnitude seems to be somewhat smaller than for the other electrocatalysts (see insets). This may be a real effect caused by a higher WC interaction with Pt due to higher WC load in the Pt-60WC/C than in the other catalyst, and evidences a somewhat higher occupancy of the Pt 5d band in this case.

Different feature were observed at -0.03 V (oxide region of Pt), as show in Fig. 5b, where the white line magnitudes for the Pt-WC materials, are consistently lower relative to that Pt/C. This indicates that the increase of the Pt 5d band vacancy caused by the oxide formation on Pt is less pronounced for the Pt-carbide materials, evidencing smaller Pt-oxide coverage. This observation is consistent with the decrease of the desorption free energy of Pt-OH, Pt-O or Pt-O_2, due to the presence WC/C, as evidenced by cyclic voltammetry.

In summary, the present results confirm the existence of specific interaction of the Pt particles with the WC/C substrates, which favor a decrease of the desorption free energy of Pt-OH, Pt-O or Pt-O_2, so that the reduction of adsorbed oxygen intermediate becomes more facile. On the basis of these facts one would expected that the Pt-carbide materials should present higher catalytic activity for the ORR compared to Pt/C, and this was confirmed experimentally by the results in Fig. 4 and Table 3.

4. Conclusions

Tungsten carbides, with and without Pt nanoparticles, prepared by a sonochemical method, were used as catalysts for the ORR in alkaline electrolyte. Results confirmed that the samples are mixtures of mono-tungsten carbide (WC) and di-tungsten carbide (W_2C) and that these are present in nanocrystalline forms. XRD

and TEM indicated Pt particle sizes of 3.0, 5-7 and 5-9 nm for Pt/C, Pt-20WC/C and Pt-60WC/C, respectively, clearly denoting higher Pt particle sizes (low surface areas) in the Pt-carbide materials.

Cyclic voltammograms confirmed the smaller Pt surface areas for the Pt-carbide materials and also evidence a decrease of the desorption free energy of Pt-OH, Pt-O or Pt-O_2, due to the presence WC/C. Steady-state polarization curves for the oxygen reduction on the Pt-60WC/C and Pt-20WC/C electrocatalysts evidenced that the onset potential of the ORR shifted to more positive values by around 50 mV and 30 mV, respectively, compared to Pt/C, indicating the higher activity of these materials. XANES results for the PtWC-based materials evidenced an increase of the Pt 5d band occupancy, and this leads to a weaker Pt-OH_x interaction, resulting in a lower Pt-oxide coverage as also shown by CV, so increasing the kinetics of the ORR.

Acknowledgments

The authors thank CNPq, Capes and FAPESP for financial support and LNLS (Brazilian National Laboratory of Synchrotron Light) for the XANES analyses.

References

[1]W. Vielstich, A. Lamm, H. A. Gasteiger, Handbook of Fuel Cells: Fundamentals Technology and Applications; Wiley: West Sussex, U.K (2003).

[2]T. Ghosh, M. B. Vukmirovic, F. J. DiSalvo, R. R. Adzic, J. Am. Chem. Soc. 132 (2010) 906.

[3]K. Kinoshita, Electrochemical Oxygen Technology, John Wiley & Sons, New York (1992).

[4]F. H. B. Lima, J. Giz, E. A. Ticianelli, J Braz. Chem. Soc. 16 (2005) 328.

[5]T. Toda, H. Igarashi, M. Watanabe, J. Electroanal. Chem. 460 (1999) 258.

[6]S. Mukerjee, S. Srinivasan, M. P. Soriaga, J. McBreen, J. Phys. Chem. 99 (1995) 4577.

[7]X. Yang, Y. C. Kimmel, J. Fu, B. E. Koel, J. G. Chen, ACS Catal. 2 (2012) 765.

[8]M. C. Weidman, D. V. Esposito, Y. C. Hsu, J. G. Chen, J. Power Sources 202 (2012) 11.

[9]Y. Wang, C. He, A. Brouzgou, Y. Liang, R. Fu, D. Wu, P. Tsiakaras, S. Song, J. of Power Sources 200 (2012) 8.

[10]D. J. Ham, C. Pak, G. H. Bae, S. Han, K. Kwon, S. Jin, H. Chang, S. H. Choi, J. S. Lee, Chem. Commun. 47 (2011) 5792.

[11]Z. J. Mellinger, T. G. Kelly, J. G. Chen, ACS Catal. 2 (2012) 751.

[12]D. V. Esposito, J. G. Chen, Energy Environ. Sci. 4 (2011) 3900.

[13]D. Meza, U. Morales, P. Roquero, L. Salgado, Int. J. Hydrogen Energy 35 (2010) 12111.

[14]Y. Liu, W. E. Mustain, ASC Catal. 1 (2011) 212.

[15]W. Zhu, A. Ignaszak, C. Song, R. Baker, R. Hui, J. Zhang, F. Nan, G. Botton, S. Ye, S. Campbell, Electrochim Acta 61 (2012) 198.

[16]S. Yin, M. Cai, C. Wang, P. K. Shen, Energy Environ. Sci. 4 (2011) 558.

[17]H. Meng, P. K. Shen, Chem Commun, (2005) 4408.

[18]M. Nie, P. K. Shen, Z. Wei, J. Power Sources 167 (2007) 69.

[19]X. Zhou, Y. Q. Yu, J. Yu, J. Yin, S. Gao, Int. J. Hydrogen Energy 36 (2011) 7398.

[20]M. Nie, P. K. Shen, Z. Wei, Q. Li, H. Bi, C. Liang, ECS Electrochem. Lett 1 (2012) 11.

[21]N. R. Elezovic, B. M. Babic, Lj. Gajic-Krstajic, P. Ercius, V. R. Radmilovic, N. V. Krstajic, Lj. M. Vracar, Electrochim. Acta 69 (2012) 239.

[22]M. Shao, B. Merzouguia, K. Shoemaker, L.Stolar, L. Protsailo, Z. J. Mellingerb, I. J. Hsub, J. G. Cheng, J. Power Sources 196 (2011) 7426.

[23]T. Hyeon, M. Fang, K. S. Suslick, J. Am. Chem. Soc. 118 (1996) 5492.

[24]A. Löfberg, A. Frennet, G. Leclercq, L. Leclercq, J. M. Giraudon, J. Catal. (2000) 189.

[25]A. L. N. Pinheiro, A. Oliveira-Neto, E. C. de Souza, J. Perez, V. A. Paganin, E. A. Ticianelli, E. R. Gonzalez, J. New Mater. Electrochem. Syst. 6 (2003) 1.

[26]A. R. West, in Solid State Chemistry and Its Applications, John Wiley & Sons, New York (1984).

[27]G. A. Camara, M. J. Giz, V. A. Paganin, E. A. Ticianelli, J. Electroanal. Chem. 537 (2002) 21.

[28]F. H. B. Lima, E. A. Ticianelli, Electrochim. Acta 49 (2004) 4091.

[29]A. Damjanovic, M. A. Genshaw, O. M. Bockris, J. Electrochem Soc. 114 (1976) 1107.

[30]W. J. Albery, M. L. Hitchman, *in Ring-Disc Electrodes,* Oxford University Press, Oxford, 17-28 (1971).

[31]L. Geniès L, R. Faure, R. Durand, Electrochim. Acta 44 (1998)1317.

[32]J. McBreen, W. E. O. Grady, K. I. Pandya, R. W. Roffman, D. E. Sayers, Lagmuir. 3 (1987) 428.

[33]P. M. Patterson, T. K. Das, B. H. Davis, Appl. Catal. 251 (2003) 449.

[34]J. Clavilier, D. Armand, B. L. Wu, J. Electroanal. Chem. 135 (1982) 159.

[35]J. Perez J, E. R. Gonzalez, E. A. Ticianelli, Electrochim. Acta 44 (1998) 1329.

[36]F. H. B. Lima, J. F. R. de Castro, E. A. Ticianelli, J. Power Sources 161 (2006) 806.

[37]J. Zhang, Y. Mo, M. B. Vukimirovic, R. Klie, K. Sasaki, R. R. Adzic, J. Phys. Chem. B 108 (2004) 10955.

[38] O. Y. Khyzhun, J. Alloys Compd. 305 (2000) 1.

Figure Captions

Figure 1: XRD patterns for Pt/C and WC-based catalysts.

Figure 2: TEM images of the WC-based catalysts. a) Pt-20WC/C and b) Pt-60WC/C.

Figure 3: Cyclic voltammograms recorded from WC-based electrocatalysts at 50 mVs^{-1} in 1.0 M KOH. Electrode geometric area: 0.196 cm^2.

Figure 4: Oxidation current in the ring and the steady-state polarization curves for the oxygen reduction on the disk produced at 5.0 mV s^{-1} in 1.0 M KOH at ω = 1600 rpm. Electrode geometric area: 0.196 cm^2.

Figure 5: XANES spectra for PtWC-based electrocatalysts at the Pt L_3 edge at (a) -0.3 V and (b) -0.03 V. Inset in (a) and (b): magnified detail of the white line.

Table 1: Crystallite sizes, lattice parameters and surface areas obtained from the voltammetric curves, transmission electron microscopy and XRD for the Pt-WC catalysts

Catalysts	d_{TEM} (nm)	d_{XRD} (nm)	*Lattice Paramenter (nm)*	Active area from CV (cm^2)	Area XRD (cm^2)	Active area TEM (cm^2)
Pt/C 20% E-Tek	3.0	3.0	0.3931	11.6	38	38
Pt-60WC/C	9.0	5.3	0.3916	7.6	23	13
Pt-20WC/C	7.0	5.0	0.3915	3.6	23	16

Table 2: Kinetic parameters and relative amount HO_2^- of different electrocatalysts

Catalyst	n_t	x^m/%	*onset* potential ORR (V)
Pt/C E-Tek	3.7	0.46	0.01
Pt-60WC/C	3.9	0.45	0.06
Pt-20WC/C	3.5	0.50	0.04
60WC/C	2.5	65.0	- 0.11
20WC/C	2.7	25.0	- 0.15
Vulcan Carbon	2.2	91.0	- 0.16

Table 3: Specific Activity (SA) calculated at -0.076 and -0.026 V vs. $Hg/HgO/OH^-$ for the Pt-based electrocatalysts.

Catalyst	$SA_{-0.076\ V}$ / mA cm^{-2}	$SA_{-0.026\ V}$ / mA cm^{-2}
Pt/C	1.82	0.29
Pt-60WC/C	2.61	1.44
Pt-20WC/C	2.28	0.80

Figure 1

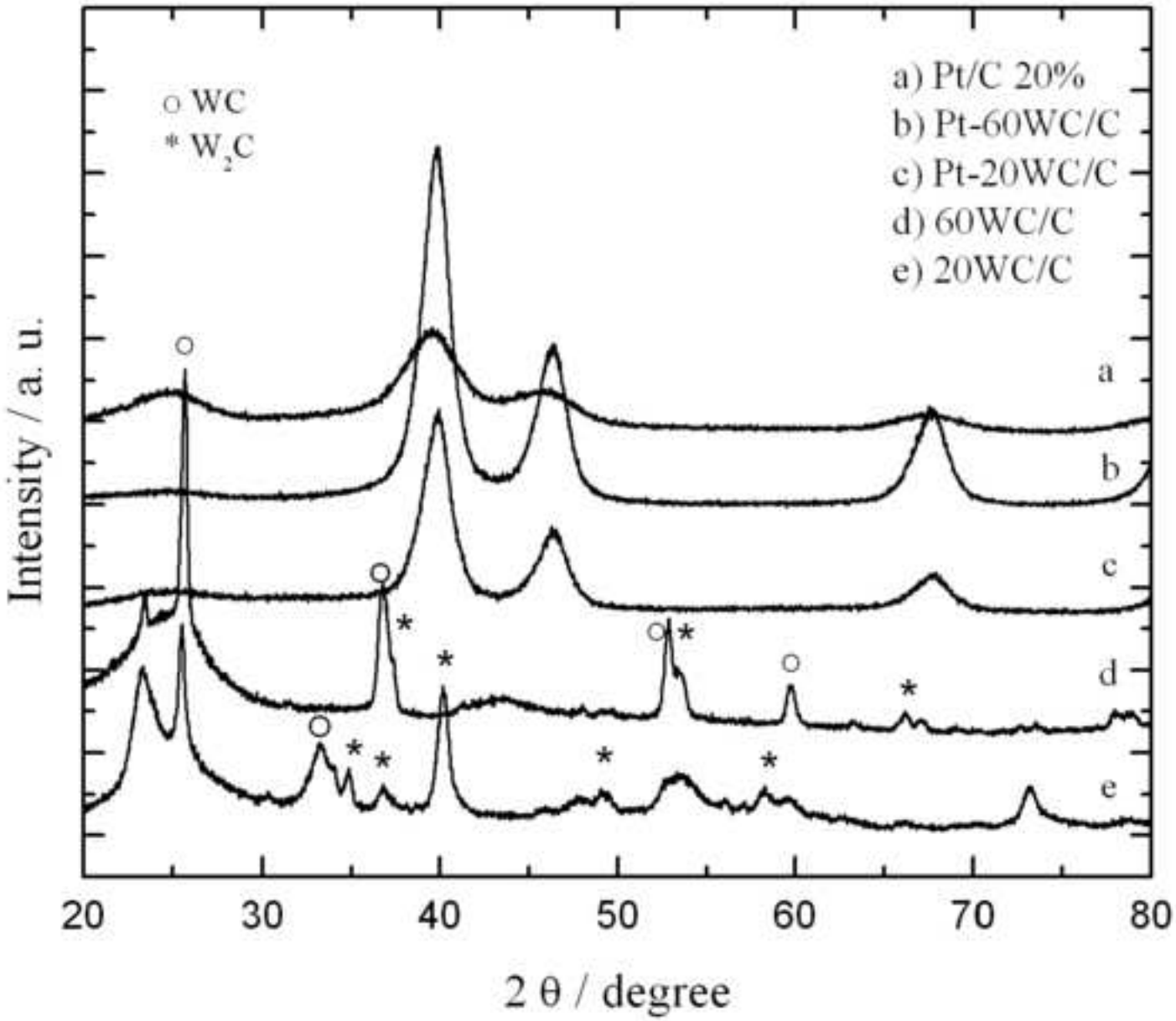
○ WC
* W2C
a) Pt/C 20%
b) Pt-60WC/C
c) Pt-20WC/C
d) 60WC/C
e) 20WC/C
Intensity / a. u.
2 θ / degree
20
30
40
50
60
70
80
a
b
c
d
e

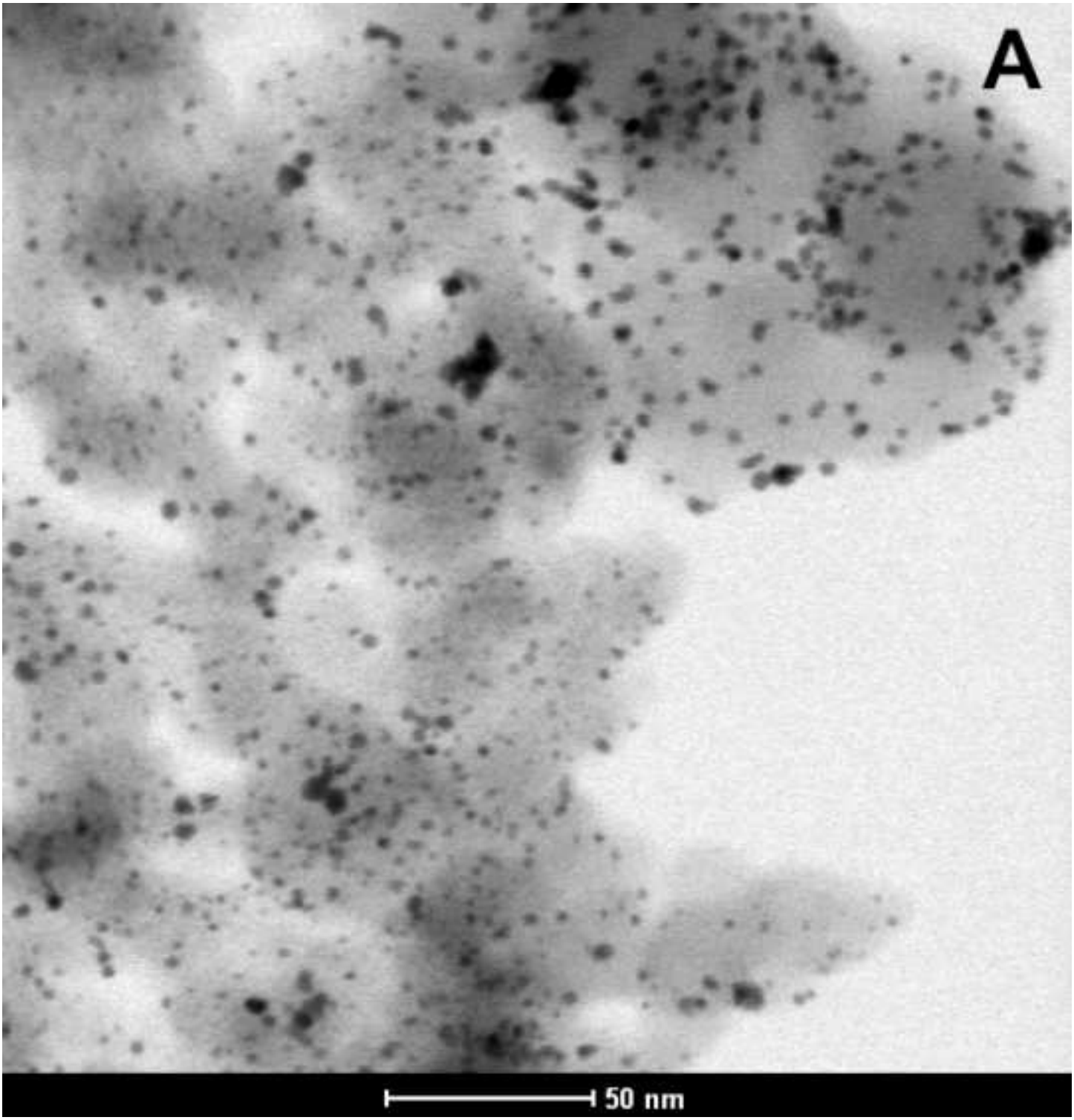

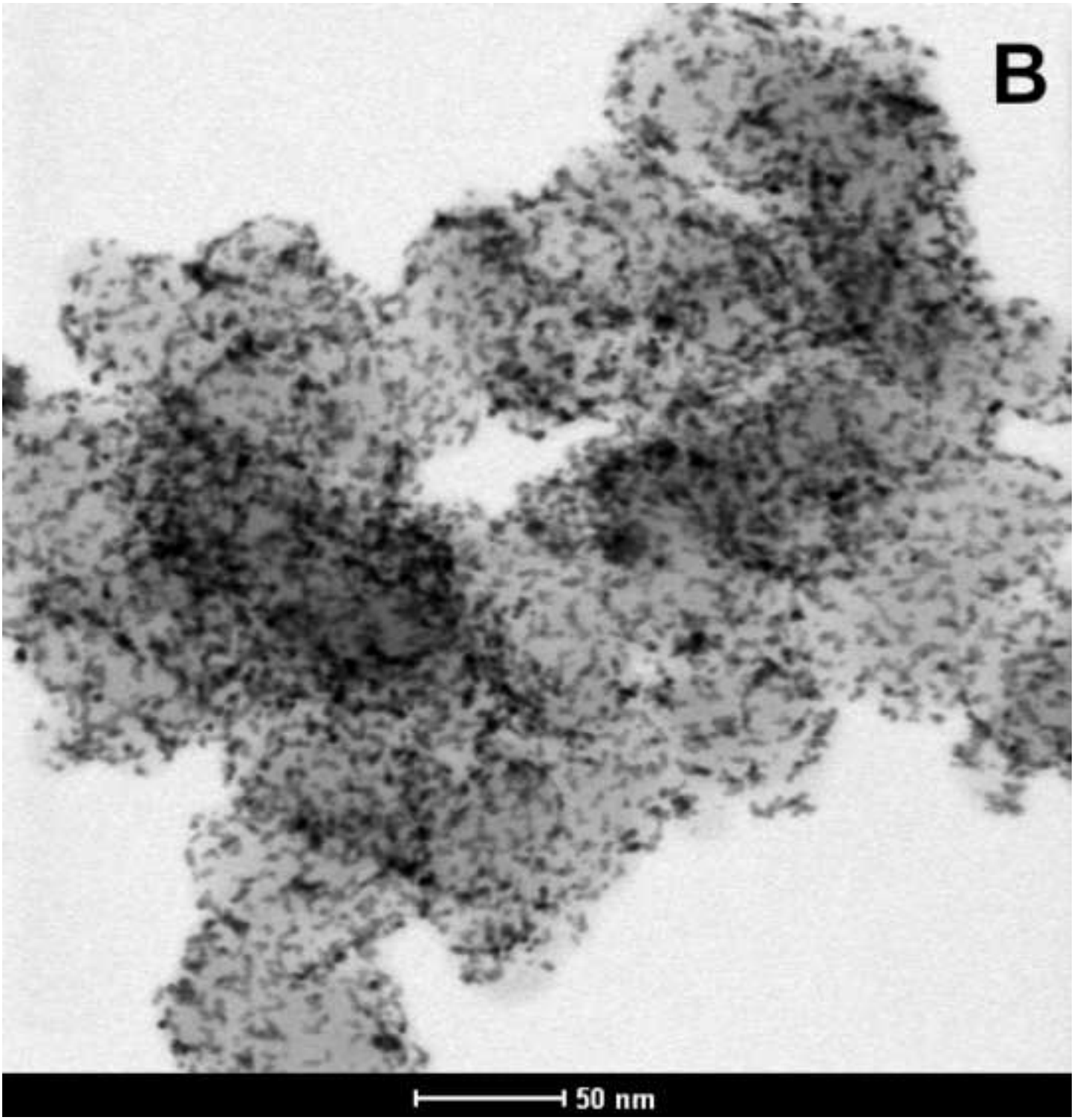

Figure 3

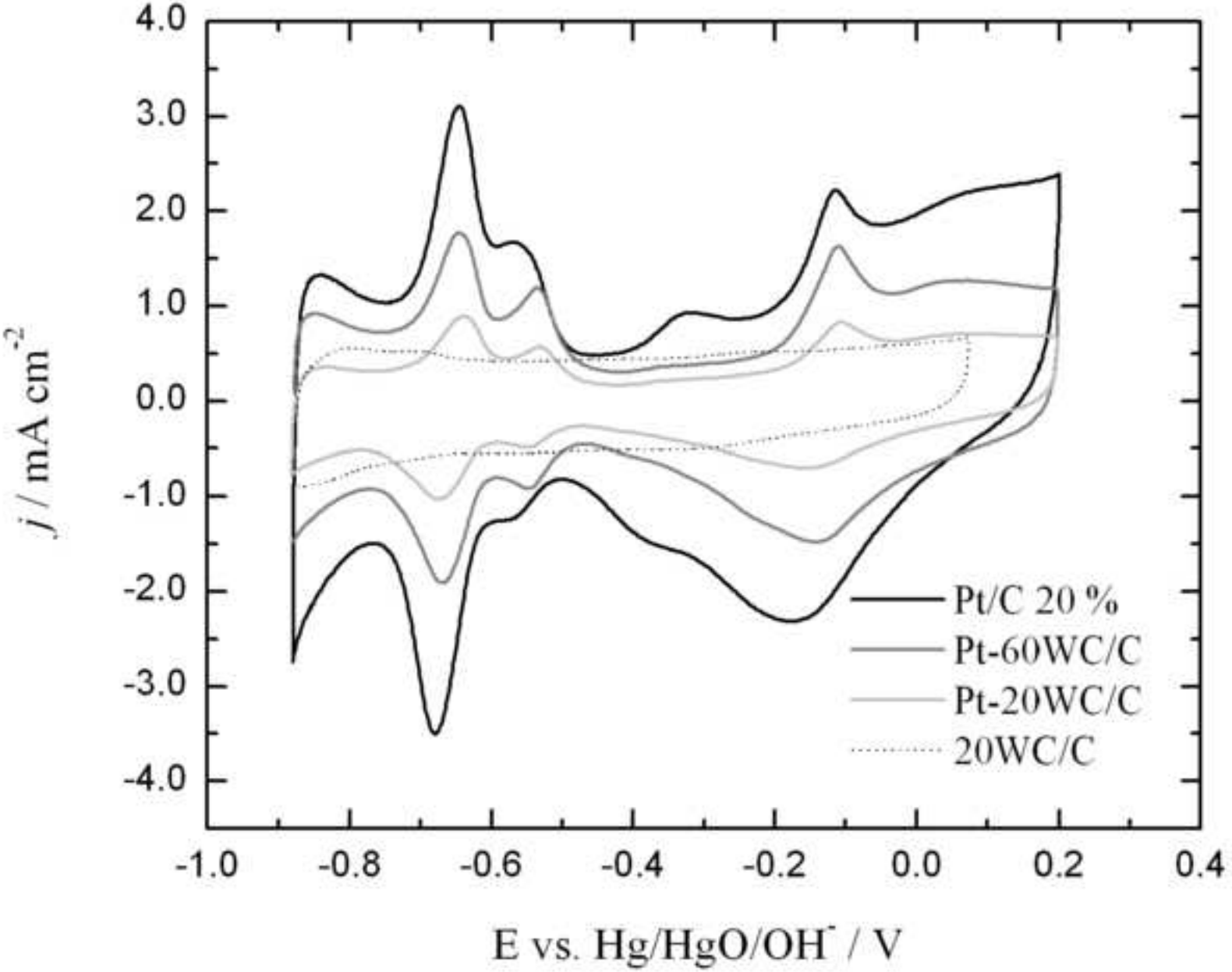
4.0
3.0
2.0
1.0
0.0
-1.0
-2.0
-3.0
-4.0
j / mA cm-2
-1.0
-0.8
-0.6
-0.4
-0.2
0.0
0.2
0.4
E vs. Hg/HgO/OH- / V
Pt/C 20 %
Pt-60WC/C
Pt-20WC/C
20WC/C

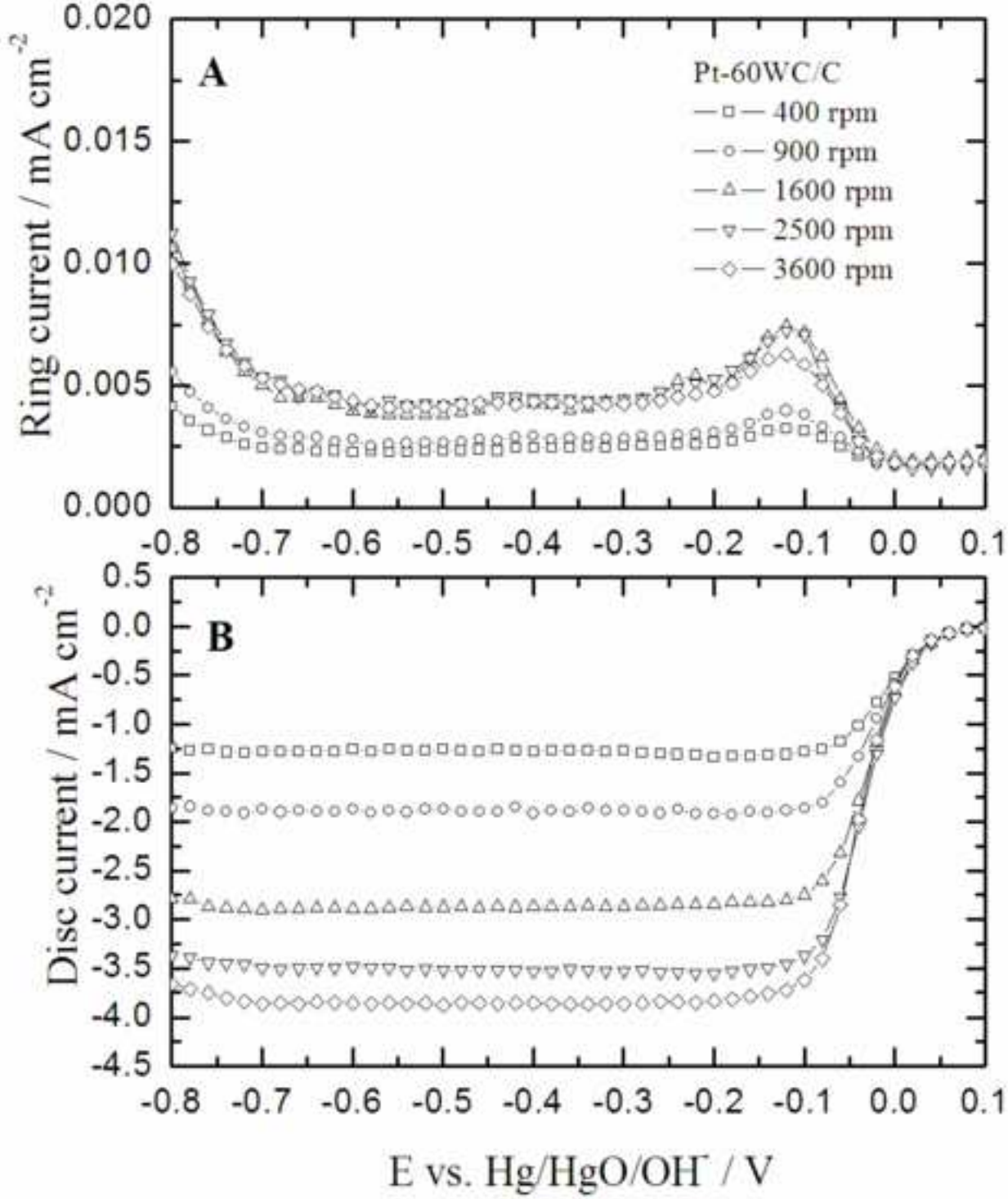

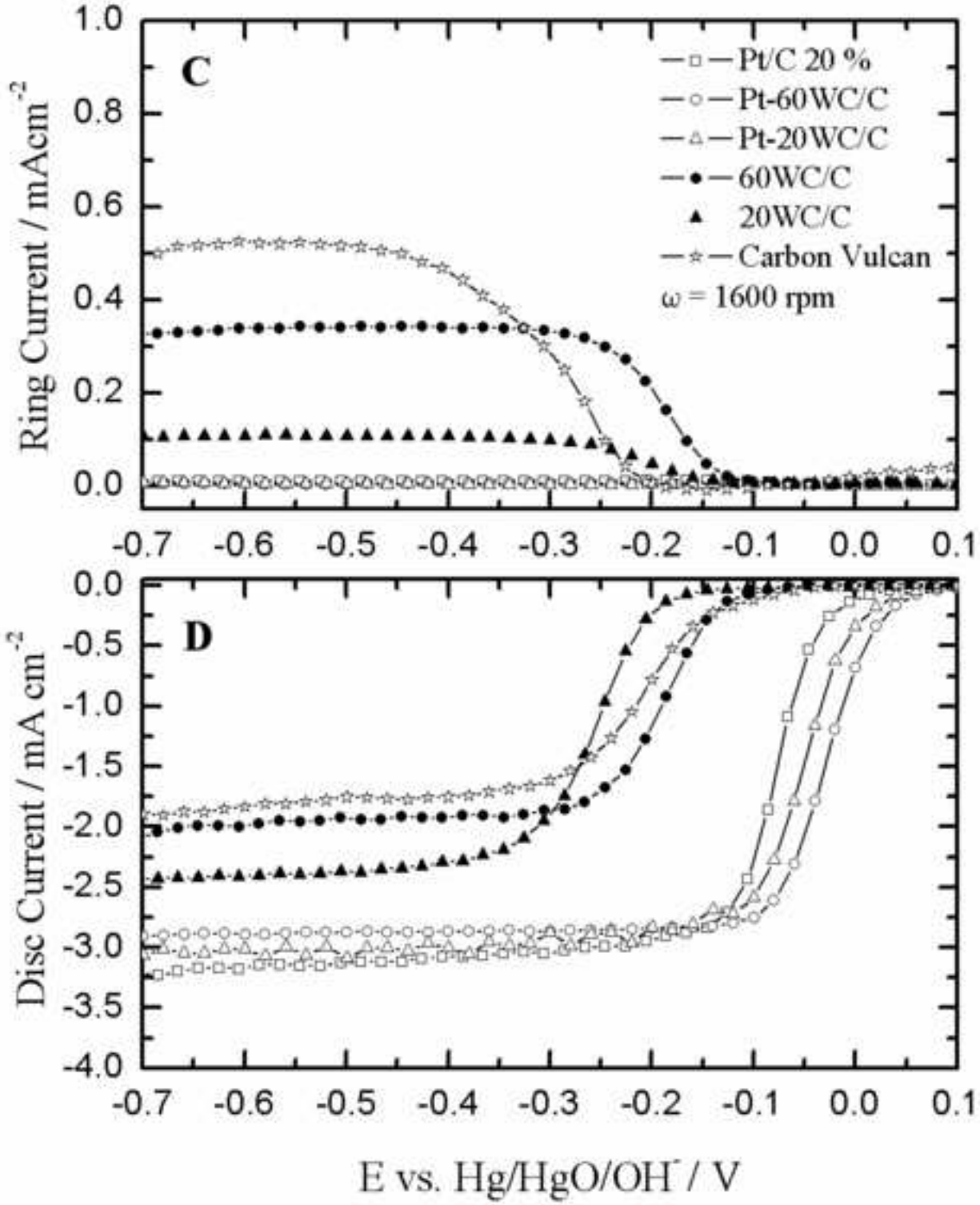

Figure 5a

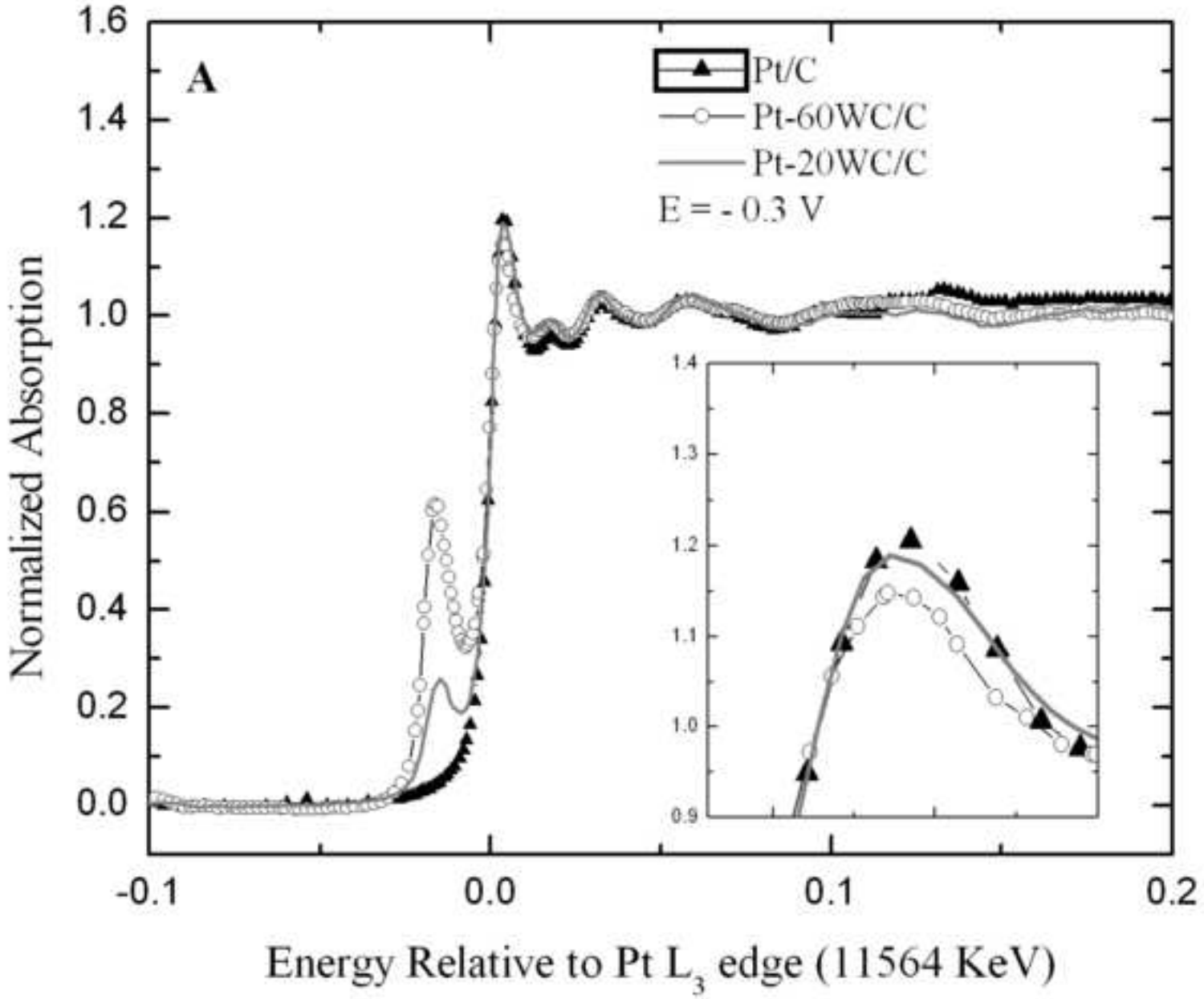
A
Pt/C
Pt-60WC/C
Pt-20WC/C
E = - 0.3 V
Normalized Absorption
Energy Relative to Pt L3 edge (11564 KeV)
1.6
1.4
1.2
1.0
0.8
0.6
0.4
0.2
0.0
-0.1
0.0
0.1
0.2
1.4
1.3
1.2
1.1
1.0
0.9

Figure 5b

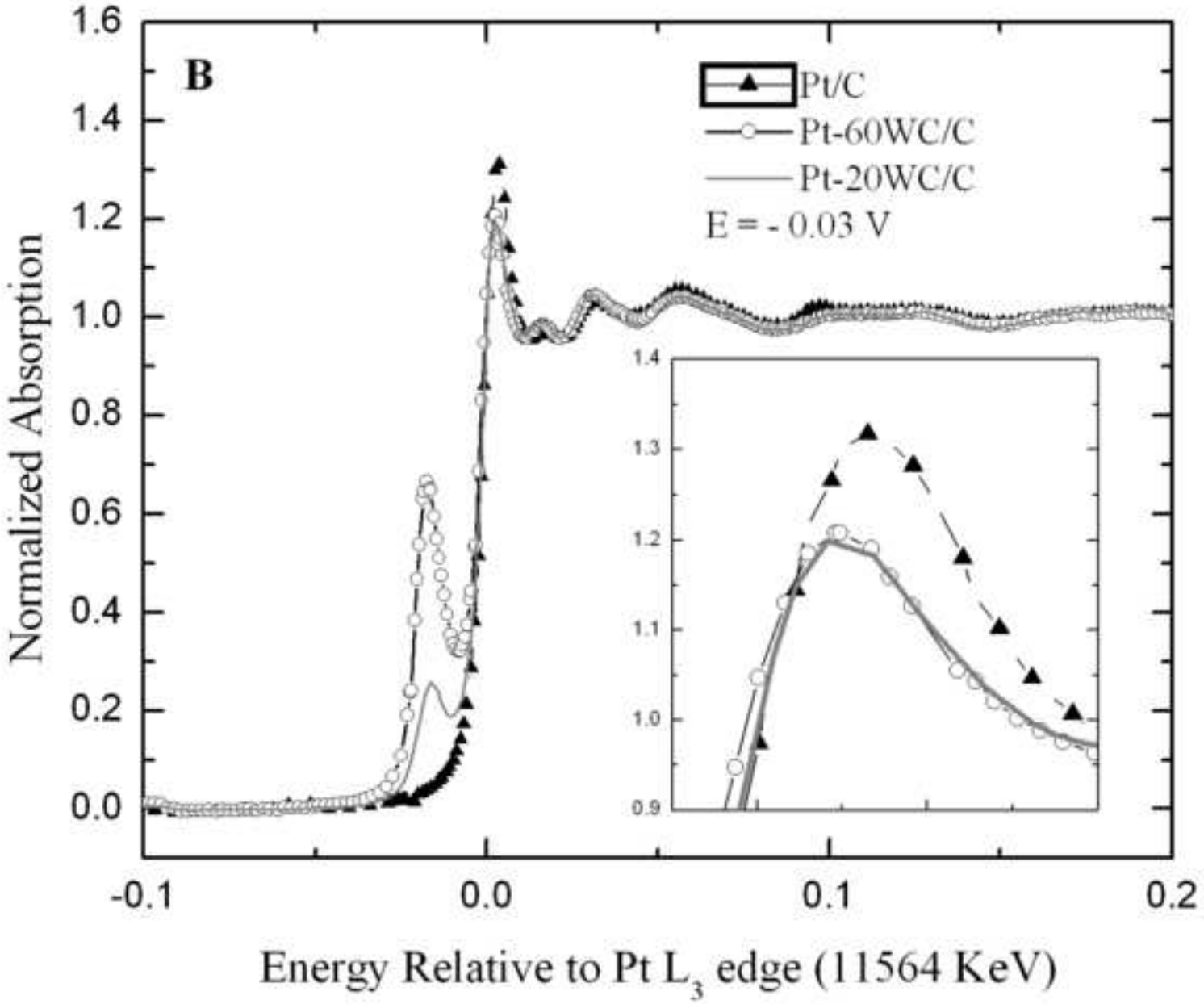
B
Pt/C
Pt-60WC/C
Pt-20WC/C
E = - 0.03 V
Normalized Absorption
Energy Relative to Pt L3 edge (11564 KeV)
1.6
1.4
1.2
1.0
0.8
0.6
0.4
0.2
0.0
-0.1
0.0
0.1
0.2
1.4
1.3
1.2
1.1
1.0
0.9